Article

Asphaltene Deposition in Different Depositing Environments: Part 2. Real Oil.

Mohammad Tavakkoli, Sai Ravindra Panuganti, Vahid Taghikhani, Mahmoud Reza Pishvaie, and Walter G Chapman

Energy Fuels, **Just Accepted Manuscript** • DOI: 10.1021/ef401868d • Publication Date (Web): 15 Apr 2014

Asphaltene Deposition in Different Depositing Environments: Part 2. Real Oil.

Mohammad Tavakkoli[1, 2], Sai R. Panuganti[1], Vahid Taghikhani[2], Mahmoud Reza Pishvaie[2] and Walter G. Chapman[1]

1. Department of Chemical and Biomolecular Engineering, Rice University, Houston, USA

2. Department of Chemical and Petroleum Engineering, Sharif University of Technology, Tehran, Iran

Authors Email Address: mohammad.tavakkoli@rice.edu, sai@rice.edu, taghikhani@sharif.edu, pishvaie@sharif.edu and wgchap@rice.edu

Corresponding Author: email - wgchap@rice.edu, Phone - 001(713) 348-4900

Abstract

This article is a continuation of our previous article (Part 1) which discussed the roles of different phenomena effecting the deposition of asphaltene from model oil systems and before the onset of asphaltene precipitation. The study in this article is to understand the depositional tendency of asphaltene using a quartz crystal microbalance with dissipation measurements (QCM-D) and their corresponding modeling for real crude oil systems with emphasis after the onset of asphaltene precipitation.

Keywords: deposition, asphaltene, QCM-D, crude oil, modeling, precipitation.

1. Introduction

In our previous article (Part 1), we discussed that in order to improve asphaltene deposition mitigation technologies, knowledge of the deposition mechanism of asphaltene and the factors influencing deposition is needed for many different domains of the oil industry [1]. QCM-D experiments are performed here to study different depositional aspects of asphaltene from model oil (Part 1) and real crude oil (Part 2) systems. Though a few researchers have used

quartz crystal microbalance for investigating asphaltene adsorption kinetics, they all were limited to model oil systems. To our knowledge only Abudu and Goual used crude oil for QCM-D adsorption measurements [2]. They used crude oil in different solvents under flow conditions. In toluene, Langmuir type adsorption was recorded with saturation film thicknesses of 3-4 nm and limited desorption after rinsing. In n-alkanes (n-heptane, n-decane, and n-pentadecane), saturation plateaus were not observed within the experimental time scale. Film thicknesses recorded after 3.5 hours were all higher than those in toluene and increased with increasing n-alkane carbon number.

In our previous article (Part 1), a model is presented for the first time in literature to capture the asphaltene adsorption process in a QCM-D before the precipitation onset. However, the asphaltene depositional problems in well-bore and pipeline are also associated with asphaltene precipitation issues. Insufficient understanding of asphaltene deposition mechanisms after precipitation onset lead to only a few modeling studies being published in the literature. Ramirez et al. described the usage of a molecular diffusion model to represent asphaltene deposition assuming that the particle concentration gradient is caused by the temperature gradient at the wall [3]. But, the asphaltene deposition rate is not affected by the temperature gradient [4]. Jamialahmadi et al. developed an experimental setup to measure the thickness of asphaltene deposit based on change in resistivity of the boundary layer [5]. Their mechanistic model for asphaltene deposition failed to take into account the aggregation process. Zhu et al. performed three phase computational fluid dynamic calculations for determining the asphaltene deposition and concluded that deposition in bend and sudden changed pipelines is greater than that in straight ones [6].

Sileri et al. focused on modeling of asphaltene deposition in crude preheat train [7]. This is the only work which incorporated aging phenomena of asphaltene (even though empirical). Nevertheless, their focus was on displacement and removal of an initial uniformly distributed layer of deposit at the walls. Recently, Eskin et al. used particle flux mass transfer expressions for turbulent flows to model the deposition process [8]. The required model parameters are obtained by fitting the model predictions to the deposition results obtained from their coquette flow device. Vargas et al. proposed a deposition simulator based on species conservation coupled with thermodynamic modeling of oil with PC-SAFT [9]. A capillary scale setup was used to estimate the parameters required in the model. The work by Vargas et al. was extended and developed into a field scale computationally efficient deposition simulator called the asphaltene deposition tool (ADEPT) by Kurup et al. who discussed asphaltene deposition in a few field cases [10, 11].

This paper investigates crude oil asphaltene-surface interactions through characterization of the deposition behavior on various surfaces using QCM-D under flow conditions. The main surface type used for experiments involving crude oil is carbon steel. Different mathematical models are used to model the experimental data obtained in this study for before and after the asphaltene precipitation onset, because of the different deposition mechanisms before and after precipitation. The effect of surface type on the deposition after precipitation is discussed based on carbon steel, iron oxide and gold sensors. Throughout the manuscript ‘Part 1’ article refers to our previous manuscript [1], and ‘Part 2’ article refers to the current manuscript.

2. Experimental Procedures

For this article, experiments are conducted to investigate the deposition behavior of asphaltene on metal surfaces from crude oil. The same crude oil (S) used for extracting

asphaltene to prepare model oil solutions in 'Part 1' article is used here directly. Table 1 shows the properties of crude oil (S). The experimental procedures for asphaltene adsorption experiments using QCM-D and determination of asphaltene precipitation onset have already been described in our previous article (Part 1). The same equipment, parts and set up from model oil study (Part 1) are retained for QCM-D study with crude oils.

Table 1. Crude oil (S) properties at 1 atmosphere and 20 ^{o}C.

Property	Value
Density (g/cc)	0.843
Molecular Weight (g/mol)	193
Viscosity (cP)	9.5
Saturates (wt%)	66.26
Aromatics (wt%)	25.59
Resins (wt%)	5.35
n-C_5 Asphaltene (wt%)	2.80

In this study, using crude oil directly eliminates the need for asphaltene extraction. All the reagents used here are HPLC grade and procured from Sigma-Aldrich. All experimental solutions are freshly prepared before the start of the experiment. Before preparing the solutions, crude oil is filtered using a 0.2 μm Nylon filter paper to remove undesirable large particles which can plug the flow system.

Unlike model oils where solvents of known properties are used, the density and viscosity of crude oil solutions had to be measured for deposition modeling purposes. Dynamic viscosity is calculated from kinematic viscosity measurements using a calibrated Cannon-Fenske viscometer of size 50. The method involves measuring the flow time of Newtonian liquids in a capillary with an accuracy of 1 second. A glass pycnometer with 5 ml capacity is used to measure the liquid density.

3. Modeling

3.1. Frequency and Dissipation Changes

In QCM-D experiments, interpreting the frequency and dissipation changes (Δf and ΔD respectively) in terms of mass/thickness and properties of the deposit have already been discussed in our previous article (Part 1) [1]. Figure 1 presents frequency and dissipation changes versus time for the adsorption of asphaltene from crude oil + n-heptane + toluene system (10:70:20) onto a carbon steel crystal surface. Δf and ΔD in Figure 1 represent an adsorbed viscoelastic film because of the following observation.

- Spreading of the overtones in Δf and ΔD responses.
- $|\Delta D/\Delta f|$ is comparable to $0.4 \times 10^{-6}\ Hz^{-1}$ [12].

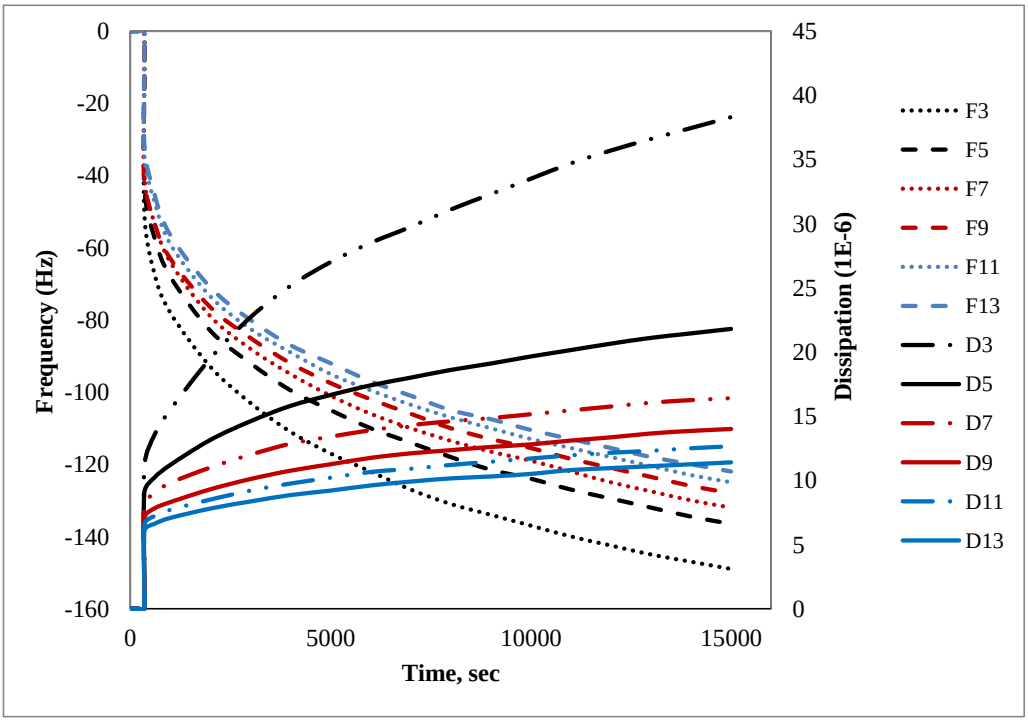

Figure 1. Frequency and dissipation changes versus time for the adsorption of asphaltene from crude oil + n-heptane + toluene system (10:70:20) onto a carbon steel crystal surface at 20 ^{o}C.

In this study, all experiments for crude oil plus heptol (mixture of n-heptane and toluene) showed viscoelastic behavior for the deposited asphaltene layer on to a crystal surface. Hence, the Voigt model, available in the Q-tools software from Q-sense, is used for viscoelastic interpretation of frequency and dissipation changes. The resultant deposited mass is treated as experimental data like all other QCM-D experiments in literature.

3.2. Adsorbed Mass Modeling Before Onset

In this paper the term "Deposition" is used in general for any process of asphaltene adhesion onto a solid surface. Before asphaltene precipitation onset, where all asphaltene are stable in the system, the term "Adsorption" may also be used. After precipitation onset, only the term "Deposition" is used throughout the manuscript.

In our previous article (Part 1) a kinetic-diffusive-convective model is presented and used for QCM-D asphaltene adsorption modeling (from model oil) before the precipitation onset. The same model is applied here for asphaltene adsorption from crude oil solutions. The model is based in part on the equations proposed by Filippov [13].

3.3. Deposited Mass Modeling After Onset

The mechanism of adsorption before and after the asphaltene precipitation onset is different, because of the effects of precipitation and aggregation of the precipitated asphaltene coming into picture after the onset. Hence, the model proposed in our previous article (Part 1) for asphaltene adsorption before the onset cannot be used after the precipitation has occurred. For this study, the mechanism proposed by Vargas et al. for asphaltene deposition in capillary scale experiments is utilized here for QCM-D experiments [9].

After asphaltene precipitation, the transport of asphaltene over the crystal in the flow module may follow a multistep process, including precipitation, aggregation, advection, diffusion and deposition. The mechanism is summarized pictorially in Figure 2. According to the mechanism, asphaltene precipitation leads to the appearance of primary particles, represented in Figure 2 as small dark circles. These particles can stick to one another undergoing an aggregation process, forming bigger particles, or can follow a diffusion mechanism to the surface of the crystal, where they can adhere to the surface and build up a deposit. Additionally, all particles are transported in the flow direction by the advection process. The flow is in laminar regime and the Peclet number is very high for all the QCM-D experiments studied here.

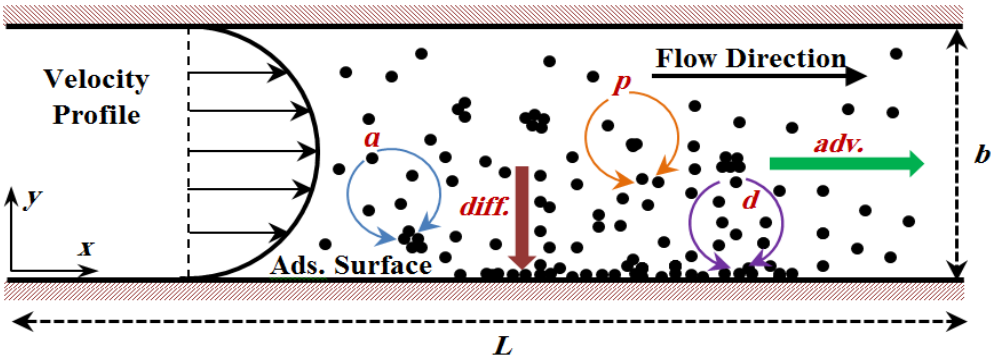

Figure 2. Mechanism of asphaltene deposition in a QCM-D flow module;

adv.: advection, *diff.*: diffusion, *a*: aggregation, *p*: precipitation, and *d*: deposition.

All of these phenomena can be incorporated into a mathematical model that tracks the transport of primary asphaltene particles. The material balance in the transient state for these primary particles is represented by equation 1, where the rates are considered as first order.

$$\frac{\partial c}{\partial t} = -V_x(y)\frac{\partial c}{\partial x} + D\frac{\partial^2 c}{\partial y^2} + k_p(c_0 - c^{eq})exp\left(-k_p\frac{x}{\langle V_x(y)\rangle}\right) - k_{ag}c \qquad (1)$$

Subject to the following boundary and initial conditions.

$$\frac{\partial c}{\partial y} = 0 \; at \; y = \frac{b}{2}, for \; all \; x \tag{2}$$

$$c = c_i \; at \; x = 0, for \; all \; y \tag{3}$$

$$D\frac{\partial c}{\partial y} = k_d c \; at \; y = 0, for \; all \; x \tag{4}$$

$$c = c_i \; at \; t = 0, for \; all \; x, y \tag{5}$$

Where c is the asphaltene primary particle's concentration in the flow cell, x is the coordinate in the direction of flow, y is the coordinate in the direction normal to the flow, t is the time, $V_x(y)$ is the axial linear velocity and $\langle V_x(y) \rangle$ is the average axial velocity, D is the diffusion coefficient, c_0 is the concentration of asphaltene in solution at inlet conditions, c^{eq} is the concentration of dissolved asphaltene at equilibrium, k_p the precipitation rate constant, k_{ag} is the aggregation rate constant, k_d is the deposition rate constant, and c_i is the concentration of primary particles at initial conditions.

In equation 1, the rate of asphaltene precipitation, r_p, is assumed to be proportional to the supersaturation degree of asphaltene, which is defined as the difference between actual concentration of asphaltene dissolved in the oil and concentration of asphaltene at equilibrium, according to equation 6.

$$r_p = k_p(c_0 - c^{eq}) exp\left(-k_p \frac{x}{\langle V_x(y) \rangle}\right) \tag{6}$$

The rates of asphaltene aggregation and deposition, r_{ag} and r_d, are defined by equations 7 and 8, respectively.

$$r_{ag} = -k_{ag} c \tag{7}$$

$$r_d = -k_d c \tag{8}$$

The details of the mathematical model can be found in the work by Vargas et al. [9].

The proposed model is implemented in the transient form to capture the experimental data against time obtained using the QCM-D experiments. A conventional numerical technique of finite differences is used for solving the partial differential equation 1 with the corresponding conditions. The PC-SAFT equation of state is applied for calculating the concentration of dissolved asphaltene at equilibrium. Procedure for obtaining the PC-SAFT parameters for oil fractions and asphaltene is well established in the literature [14-16]. Also the PC-SAFT parameters for the crude oil (S) used in this study, are already available from the work of Panuganti et al. (crude oil A in their paper) [17].

4. Results and Discussion

In this article, a solution of crude oil in heptol (10 vol% of crude oil in 90 vol% of heptol) is used as the injection fluid into QCM-D setup. A constant value for the ratio of crude oil to heptol is applied because the effect of different ratios has already been investigated by another group [2]. The ratio of 10 to 90 for crude oil to heptol is selected because the system of 10 vol% crude oil + 90 vol% n-heptane is well into the region of asphaltene precipitation for the crude oil + heptol system, and one can easily investigate the effect of precipitating agent addition (n-heptane) beyond the precipitation onset. Later in this section, we will show that the onset of asphaltene precipitation happens near 10 vol% crude oil + 70 vol% n-heptane + 20 vol% toluene. Total asphaltene concentration is maintained constant in all the solutions of 10 vol% crude oil + 90 vol% heptol. All experiments are done at 20 ^{o}C and 80 μl/min flow rate. As shown in the *Modeling* section, all experimental results showed a viscoelastic behavior of the deposited layer from crude oil + heptol system. So, the Voigt model in the Q-Tools software is applied for deposited mass interpretation from frequency and dissipation changes of the sensor crystal.

In this study as well as in our previous article (Part 1), each experiment is done three times, and the average deposited mass is reported. As observed from Figure 1, all the experimental data is smooth. Also, the results obtained from Voigt modeling shows continuous smooth curves for the amount of the deposited mass versus time. Error bars are plotted in Figure 3 on some of the data points to show that the experiments are reasonably repeatable. In Figure 3 there are over 15,000 data points to plot error bars on all the data points. The average standard deviation of the data points with error bars is 2.33%.

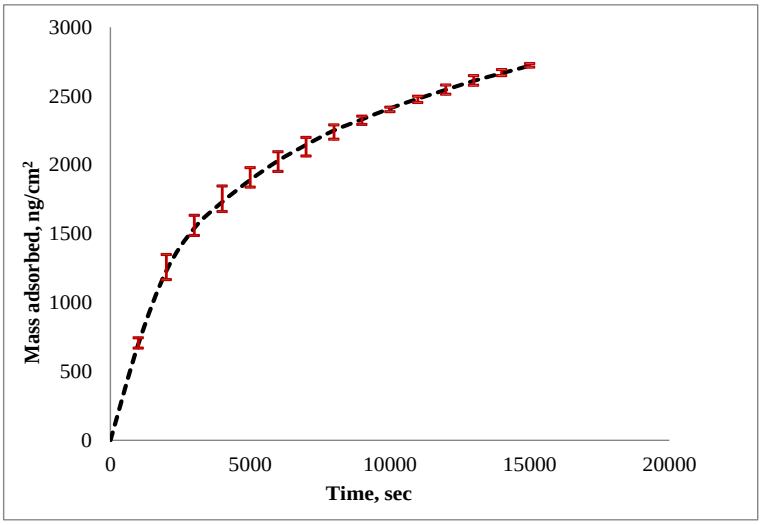

Figure 3. Adsorbed mass amount from n-C_5 asphaltene + toluene system onto a gold crystal surface versus time at 80 μL/min flow rate and 60 ^{o}C with the error bars.

4.1. Elimination of Liquid Loading Effect

Unlike model oil system (asphaltene in heptol), the viscosity and density variations caused by the introduction of crude oil into heptol imply that liquid loading effects have a non-negligible role in the QCM-D response [18]. Using equations 9 and 10, changes in both frequency and dissipation because of liquid loading effect can be calculated [18].

$$\Delta f_{liquid\ loading} = -\sqrt{\frac{n}{\pi}}\frac{f_0^{3/2}}{\rho_q v_q}\left(\sqrt{\rho_l \eta_l} - \sqrt{\rho_s \eta_s}\right) \quad (9)$$

$$\Delta D_{liquid\ loading} = -\frac{1}{\sqrt{n\pi}}\frac{2f_0^{1/2}}{\rho_q v_q}\left(\sqrt{\rho_l \eta_l} - \sqrt{\rho_s \eta_s}\right) \quad (10)$$

Where f_0 is the fundamental resonant frequency (f_0 = 5×10^6 *Hz*), n is the overtone number (n = f_n/f_0 = 1, 3, 5, 7, 9, 11 and 13), ρ_q is the specific density of quartz (2650 *kg/m*^{3}), v_q is the shear wave velocity in quartz (3340 m/s), $v_q = \sqrt{\mu_q/\rho_q} = 2f_0 h_q$, μ_q is the shear modulus of quartz (2.947×10^{10} *Pa*), h_q is the thickness of the quartz crystal (3.37×10^{-4} *m*), ρ is density, η is viscosity, and subscripts *s* and *l* refer to the solvent and liquid mixtures, respectively.

Table 2 shows the calculated $\Delta f_{liquid\ loading}$ and $\Delta D_{liquid\ loading}$ for the third harmonic overtone of 10 vol% crude oil + 90 vol% heptol system at different ratio of n-heptane to toluene. Similar calculations are performed for all other overtones, and after eliminating the effect of liquid loading from the total Δf and ΔD, one can find the net change in frequency and dissipation with time, which are due to the deposited solid particles on to the surface of the sensor crystal. Thus, Figure 4 is the resultant amount of deposited mass versus time for different ratios of n-heptane to toluene after eliminating the liquid loading effect. Liquid trapping effect is negligible because of the use of smooth sensor crystal surface.

Table 2. Calculated $\Delta f_{liquid\ loading}$ and $\Delta D_{liquid\ loading}$ for the third harmonic overtone and at different ratio of n-heptane to toluene.

Oil:Heptane:Toluene Ratio	Liquid Density (g/cc)	Liquid Viscosity (cP)	$\Delta f_{liquid\ loading}$ (Hz)	$\Delta D_{liquid\ loading}$ (× 10^{-6})
10:0:90	0.864	0.721	-30.59	12.24
10:20:70	0.828	0.645	-28.65	11.46
10:40:50	0.791	0.586	-26.24	10.50
10:60:30	0.755	0.571	-30.33	12.13
10:70:20	0.736	0.545	-28.88	11.55
10:80:10	0.718	0.536	-29.67	11.87
10:90:0	0.700	0.531	-39.42	15.77

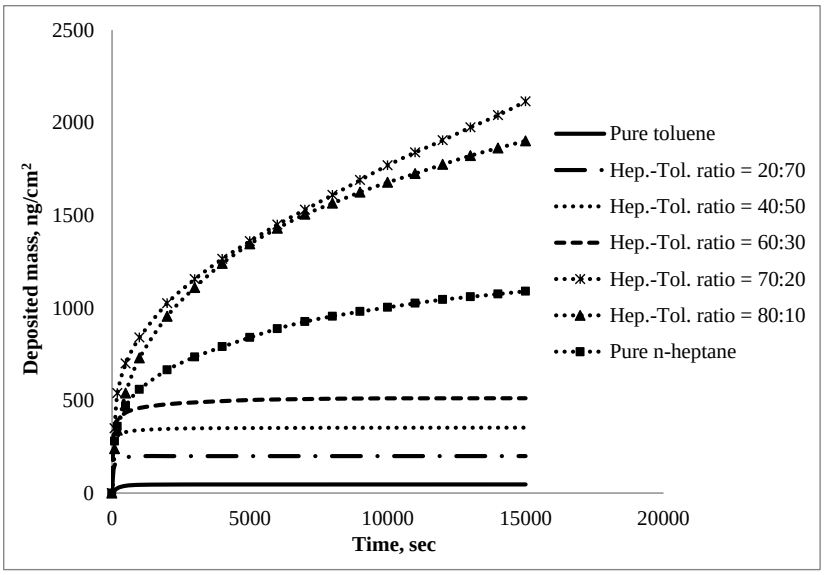

Figure 4. Deposited mass versus time from solutions of 10 vol% crude oil + 90 vol% heptol on to the surface of carbon steel sensor crystal at different ratios of n-heptane to toluene, at 20 ^{o}C and 80 μl/min flow rate after eliminating the liquid loading effects.

4.2. Modeling of Model Oil System after Onset

Our previous article (Part 1) was limited to modeling of adsorption process in a QCM-D before the precipitation of asphaltene. In this article, with the introduction of deposition modeling in a QCM-D after the precipitation of asphaltene, the model oil system is explored first before applying for real crude oil systems. As presented in our previous article (Part 1), a 100 ppm asphaltene in heptol solution resulted in Figure 5 for the deposited mass with time. Asphaltene precipitation onset for the model oil system happens near 55 volume percent of n-heptane based on the results obtained in our previous article (Part 1). From Figure 5 the maximum amount of asphaltene deposition occurs near the asphaltene precipitation onset for the model oil system. After precipitation onset, asphaltene aggregate forming larger particles which can pass over the sensor crystal surface without depositing because of convective transfer.

For calculating the concentration of dissolved asphaltene at equilibrium, c^{eq} the PC-SAFT equation of state is applied. PC-SAFT has previously shown modeling results matching experimental observations for the onset of precipitation as well as the precipitated amount from solvent-diluted crude oils at different concentrations of precipitating agents [19]. This is possible because of correct estimation of the concentration of dissolved asphaltene at equilibrium, c^{eq}. Therefore, the PC-SAFT can rightly calculate the values of c^{eq} at various concentrations of n-heptane in the both model oil and real oil systems. The calculated c^{eq} in the case of 75:25 for n-heptane to toluene ratio is 0.07482 g/m^3, and for the case of 85:15 is 0.001863 g/m^3.

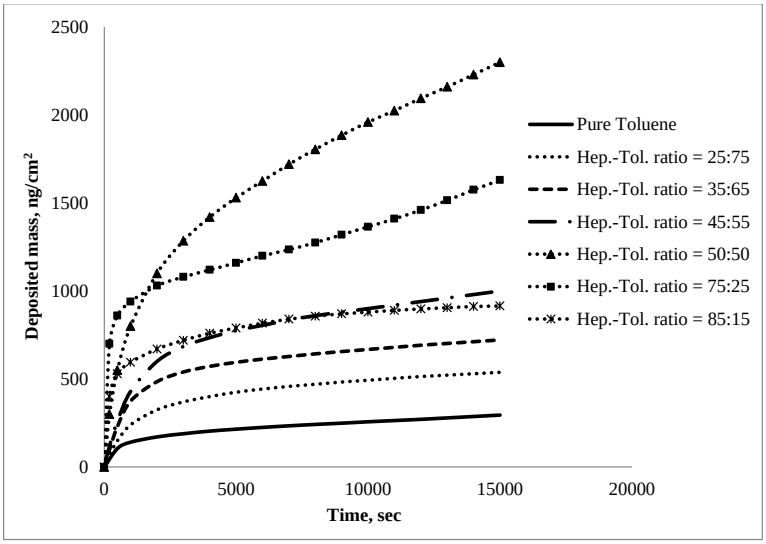

Figure 5. Deposited mass from n-C_7 asphaltene + heptol systems onto a gold crystal surface versus time at 20 ^{o}C and 80 μl/min flow rate.

Diffusion coefficient (D), kinetic constants of precipitation (k_p), aggregation (k_{ag}) and deposition (k_d) are the four adjustable parameters tuned to reproduce the experimental data for the amount of deposited mass beyond onset of asphaltene precipitation; i.e. for 75 and 85 vol% of n-heptane. These adjusted values are presented in Table 3. Figures 6 and 7 show the modeling results for the amount of deposited mass beyond asphaltene precipitation onset.

Table 3. Adjusted values of the parameters used to reproduce the experimental data for the amount of deposited mass beyond onset of asphaltene precipitation in a 100 ppm asphaltene model oil solution at 20 ^{o}C.

Parameter	75 vol% of n-heptane	85 vol% of n-heptane
D (m^2/sec)	9.00E-10	1.00E-10
k_p ($1/sec$)	2.90E-3	2.90E-3
k_{ag} ($1/sec$)	5.20E-5	5.20E-5
k_d (m/sec)	1.40E-6	1.40E-6

The operating conditions, oil, asphaltene and depositing surface are same for both the cases of 75 and 85 vol% of n-heptane in Table 3. Hence, the kinetic constants (k_p, k_{ag} and k_d) remain the same for both of them in Table 3. At constant conditions with varying oil to precipitant ratio, Kurup et al. also reported the same kinetic constant values for the different oil to precipitant ratios [11]. In Table 3 the diffusion coefficient is higher for the case of 75 vol% of n-heptane. The slightly bigger asphaltene primary particle size with increasing instability of asphaltene in solution (higher vol% of n-heptane) results in a lower diffusion coefficient [20].

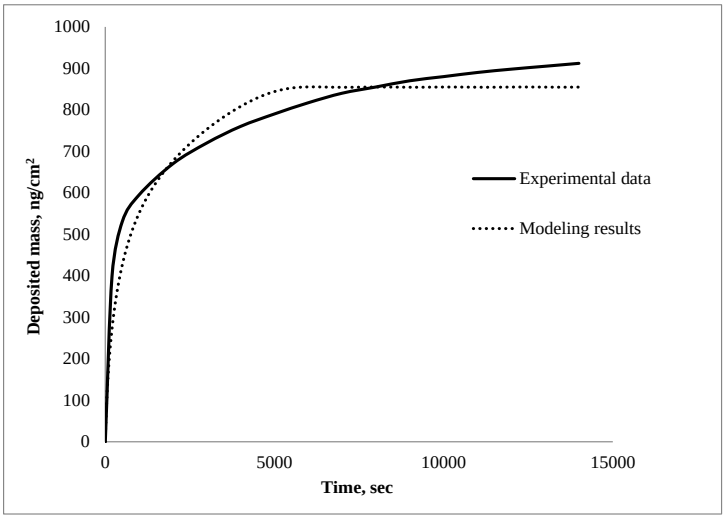

Figure 6. Experimental and modeling results of deposited mass versus time from a solution of 100 ppm n-C_7 asphaltene in heptol with 85 vol% of n-heptane on to a gold surface at 20 ^{o}C and 80 μl/min flow rate.

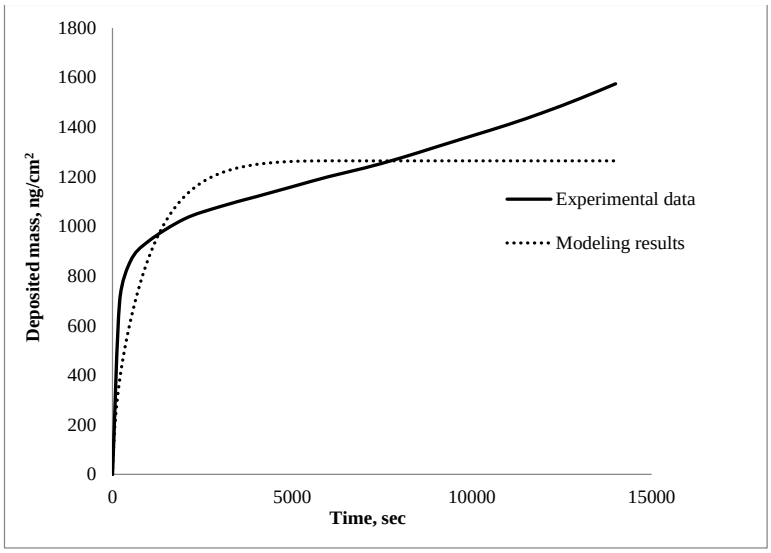

Figure 7. Experimental and modeling results of deposited mass versus time from a solution of 100 ppm n-C_7 asphaltene in heptol with 75 vol% of n-heptane on to a gold surface at 20 ^{o}C and 80 μl/min flow rate.

As mentioned in our previous article (Part 1), we could not detect when the first layer of asphaltene forms on the surface of the sensor using the QCM equipment. Before this first layer we have asphaltene-metal interactions and after forming the first layer we have asphaltene-asphaltene interactions. From modeling results, one may conclude that at initial stage of experiments where the adsorption process is controlled by the adsorption kinetics, the asphaltene-metal interactions are dominant and at long time of experiments the asphaltene-asphaltene interactions play the main role in adsorption process.

4.3. Asphaltene Precipitation Onset of Crude Oil + Heptol System

To find the onset of asphaltene precipitation, the method explained in our previous article (Part 1) is used. Figure 8 presents the absorbance as a function of heptane volume percent at 500 nm UV-Vis wavelength. The intersection of two trend lines which pass through the data points represents the volume percent of n-heptane at precipitation onset. For the crude oil (10%) +

heptol (90%) system used in this work, the precipitation onset happens near 75.18 volume percent of n-heptane based on the result obtained from Figure 8.

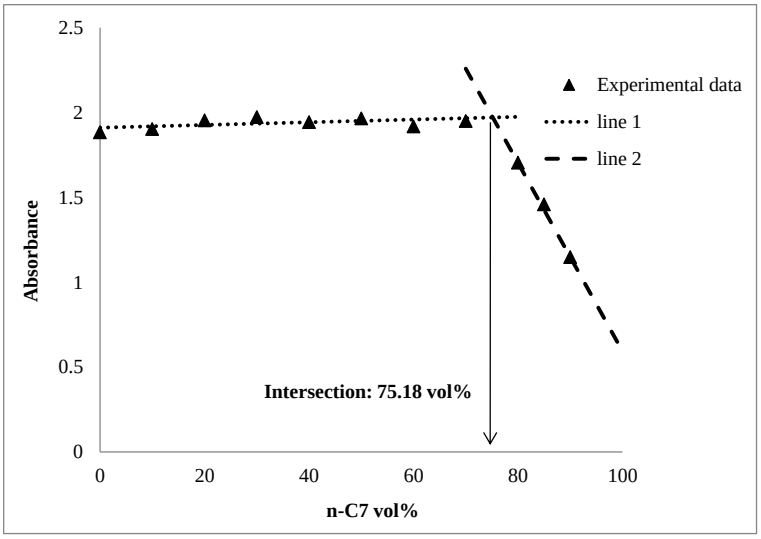

Figure 8. Precipitation onset measurement using absorbance of UV-Vis at 500 nm wavelength for the crude oil (10%) + heptol (90%) system.

Using different UV-Vis wavelengths for measuring the absorbance gives different values of the absorbance. But, the sudden deviation in the data which corresponds to volume percent of n-heptane at the precipitation onset is nearly the same. Figures 9 and 10 present the absorbance at UV-Vis wavelength of 600 and 800 nm, respectively, as a function of n-heptane volume percent. Based on the results obtained from Figures 9 and 10, the precipitation onset happens near 74.82 and 74.32 volume percent of n-heptane, respectively, which are very close to the value obtained at UV-Vis wavelength of 500 nm. The advantage of the procedure used here in obtaining the asphaltene precipitation onset without aggregation effects has already been discussed in our previous article (Part 1).

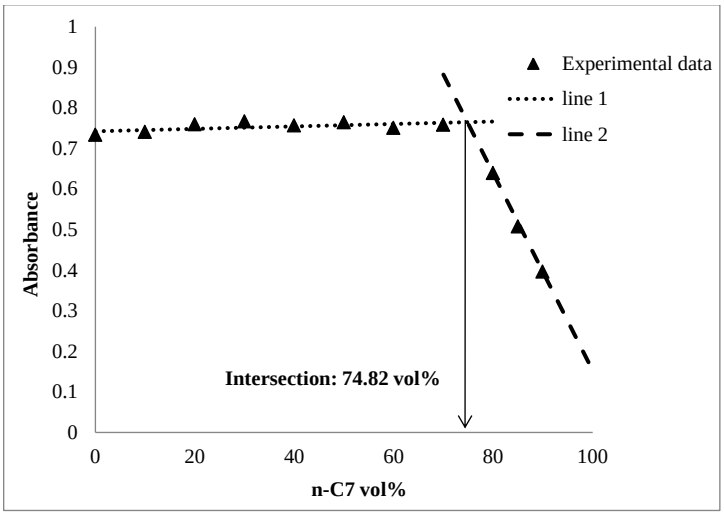

Figure 9. Precipitation onset measurement using absorbance of UV-Vis at 600 nm wavelength for the crude oil (10%) + heptol (90%) system.

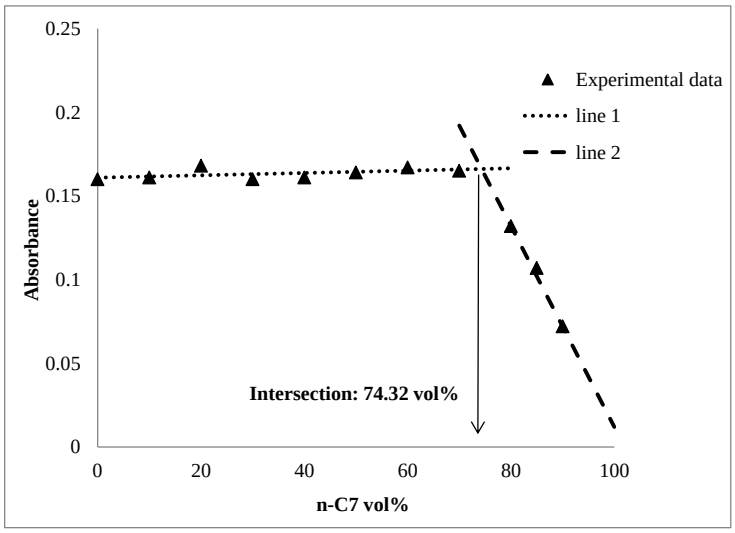

Figure 10. Precipitation onset measurement using absorbance of UV-Vis at 800 nm wavelength for the crude oil (10%) + heptol (90%) system.

4.4. Modeling of Crude Oil System before Onset

After determining the asphaltene precipitation onset for crude oil + heptol system, the QCM-D experimental data of adsorbed mass before the onset are modeled using the kinetic-diffusive-convective model described in our previous article (Part 1).

In this modeling study of the experimental data before asphaltene precipitation onset, model results showed that for initial time, the amount of mass adsorbed is a linear function of time which means that the rate of adsorption depends on K_{ad} and does not depend on parameters characterizing diffusion and convective transfer. Therefore, for this case the adsorption process is controlled by the adsorption kinetics. The adsorption process for long times is governed by the diffusion and the convective transfer. For the experimental data in Figure 4 before the onset of precipitation, all curves of deposited mass reach equilibrium very soon. Hence, Rectangular adsorption isotherm is applied to find a reasonable match. Figure 11 presents modeling results versus experimental mass adsorbed for crude oil + heptol with 60 vol% of n-heptane.

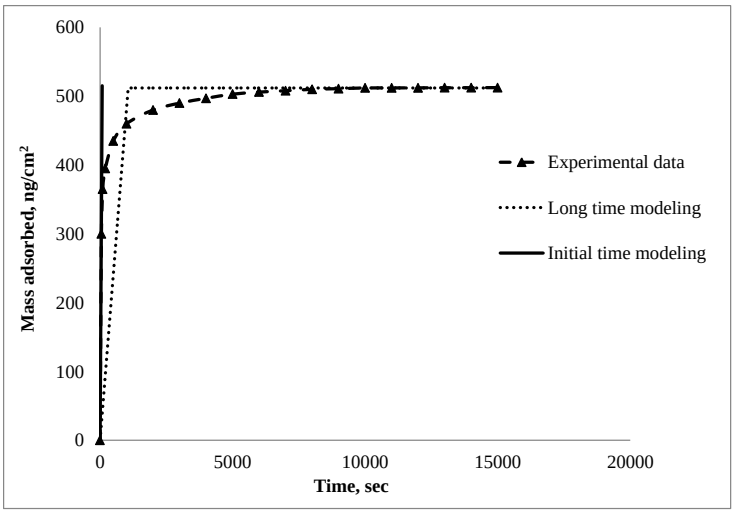

Figure 11. Experimental and modeling results for the amount of adsorbed mass from crude oil + heptol with 60 vol% of n-heptane onto a carbon steel crystal surface versus time at 20 ^{o}C and 80 µl/min flow rate.

During initial time, the values of adsorption rate constant which are used to model the amount of mass adsorbed from solutions of crude oil + heptol at 0, 20, 40, and 60 vol% of n-heptane are 0.00065, 0.0011, 0.0018, and 0.0028 per second, respectively. For long times, the diffusion coefficients of 1.0E-11, 3.5E-11, 4.2E-11, and 5.0E-11 are used at 0, 20, 40, and 60

vol% of n-heptane, respectively. Experimental temperature is constant and solution viscosity does not change much in these cases.

4.5. Modeling of Crude Oil System after Onset

For the case of crude oil (10 vol%) + heptol (90 vol%) QCM-D experimental data reported in Figure 4, when the vol% of n-heptane increases, the amount of deposited mass increases up to 70 vol% n-heptane. The amount of deposited mass decreases beyond the onset vol% of n-heptane. We believe that after asphaltene precipitation onset, the precipitated asphaltene particles aggregate forming large particles which can pass over the crystal surface without deposition because of convective transfer. The trend is captured by the model as described in this section.

For calculating c^{eq}, the concentration of dissolved asphaltene at equilibrium, the PC-SAFT equation of state is applied. The obtained c^{eq} in the case of 80 vol% of n-heptane is 53.6744 g/m^3 and for 90 vol% of n-heptane (pure n-heptane) is 1.1132 g/m^3. It should be mentioned that in these cases c^{eq} is very small in comparison to c_0 value. c_0 is around 2300 ppm for C_5 asphaltenes and somewhere below 2300 ppm for C_7 asphaltenes, but still much more than the c^{eq}. So, here we could model the deposition by assuming that we could substitute c_0-c^{eq} with c_0 and therefore avoiding SAFT beyond the precipitation onset. But, just to follow the proposed model for deposition and for being more precise, we have used c_0-c^{eq} in modeling the deposition process.

Table 4 presents the four adjustable parameters of diffusion coefficient (D), kinetic constants of precipitation (k_p), aggregation (k_{ag}) and deposition (k_d) which are tuned to reproduce the experimental data for the amount of deposited mass beyond onset of asphaltene precipitation; i.e. 80 and 90 vol% of n-heptane. Figures 12 and 13 demonstrate the modeling results for the amount of deposited mass beyond asphaltene precipitation onset.

Table 4. Adjusted values of the parameters used to reproduce the QCM-D experimental data of deposited mass beyond onset of asphaltene precipitation in crude oil + heptol solutions at 20 ^{o}C.

Parameter	80 vol% of n-heptane	90 vol% of n-heptane
D (m^2/sec)	4.50E-12	1.50E-12
k_p ($1/sec$)	6.40E-4	6.40E-4
k_{ag} ($1/sec$)	2.10E-4	2.10E-4
k_d (m/sec)	7.50E-8	7.50E-8

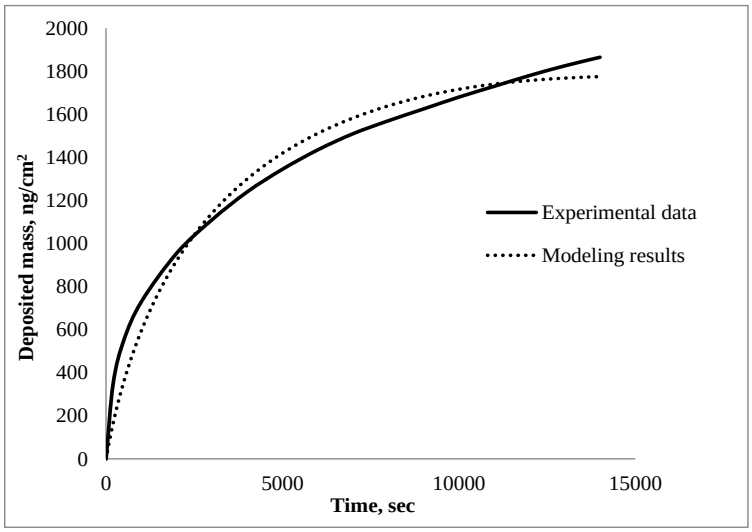

Figure 12. Experimental and modeling results of deposited mass from 10 vol% crude oil + 90 vol% heptol solution with 80 vol% of n-heptane on to a carbon steel surface at 20 ^{o}C and 80 µl/min flow rate.

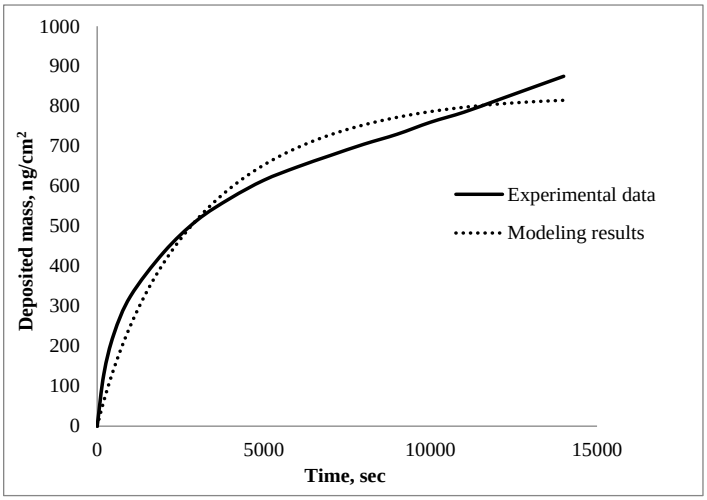

Figure 13. Experimental and modeling results of deposited mass from 10 vol% crude oil + 90 vol% heptol solution with 90 vol% of n-heptane on to a carbon steel surface at 20 ^{o}C and 80 µl/min flow rate.

In lines of the explanation presented in *Modeling of Modeled Oil System after Onset* section, comparison of the diffusion coefficient values reported in Table 4 shows a higher value for the case of 80 vol% of n-heptane than 90 vol% of n-heptane. Also, the values of kinetic constants (k_p, k_{ag} and k_d) are the same for both the cases of 80 and 90 vol% of n-heptane, because operating conditions, oil, asphaltene and depositing surface are maintained the same.

From our previous article (Part 1) it is observed that the adsorption process is mostly controlled by the kinetics of adsorption at initial time scale of the experiment. Thus the slight offset between experimental and modeling results of the deposited mass during initial time in Figures 12 and 13 is because the dissolved asphaltene particles also play a role in the adsorption process. The experimental data is accordingly a little more than the model prediction which considers only the precipitated asphaltene particles for deposition. After a long time (near 15000 sec) the model attains a saturated deposit amount, while the experimental data show that further deposition can occur (not reached saturation plateau). It should be recalled that the precipitation kinetics assumed in this work are simple first order kinetics, which may not be sufficient to describe the precipitation of the polydisperse asphaltene. Different fractions of asphaltene may precipitate out at different rates, causing the presence of deposit even after a long time.

Asphaltene concentration in the model oil is 100 ppm, while its concentration in the real oil systems is around 2.3 g/l (2300 ppm). But, the amount of deposited mass is in the same range from Figures 4 and 5. It is to be noted that the depositing surfaces are not the same for the experimental data presented in Figures 4 and 5. Also for the system with real oil, the solution is

more bulky and viscous than model oil. This results in reduced diffusion and deposition which can be justified by comparing the parameters in Tables 3 and 4.

4.6. Deposition Model Sensitivity Analysis

To understand the effect of diffusion coefficient and kinetic parameters on shape and magnitude of the asphaltene deposit profile versus time, a sensitivity analysis is performed. The parameters used to model the amount of deposited mass versus time from a solution of 10 vol% crude oil + 90 vol% heptol with 80 vol% of n-heptane, are used as the base case, and each parameter is then varied individually to understand the effect of that particular parameter on the deposition profile. The effect of k_p, k_{ag}, k_d and D on the asphaltene deposition profile are shown in Figures 14, 15, 16 and 17 respectively. The results are not clear in Figures 15 and 16 because of only small change in the deposited mass with changes in aggregation and deposition kinetic constants. Hence, Figures 18 and 19 represent the changes in deposited mass amount with higher changes of k_{ag} and k_d, respectively.

It can be seen that the value of k_p has a very significant impact on the amount of deposited mass, as compared to those of k_{ag} and k_d. A small increase in k_p shows a significant increase in the amount of deposited mass versus time, and a decrease of k_p results in decrease of deposited mass amount. Similar trends can be observed for increase and decrease in the values of diffusion coefficient, D, and deposition kinetic constant, k_d, as expected from the mechanism. A reverse trend is observed for change in k_{ag}. When k_{ag} increases, the tendency of primary asphaltene particles to aggregate and form larger particles increases. So, we have more numbers of larger particles which can pass over the crystal surface without deposition because of convective transfer, and as a final result we will have less amount of deposited mass versus time. It can be observed from Figure 18 that the effect of changes in k_{ag} on the deposited mass amount

at initial time scale is negligible, while the effects of changes in k_p and k_d are significant for all times.

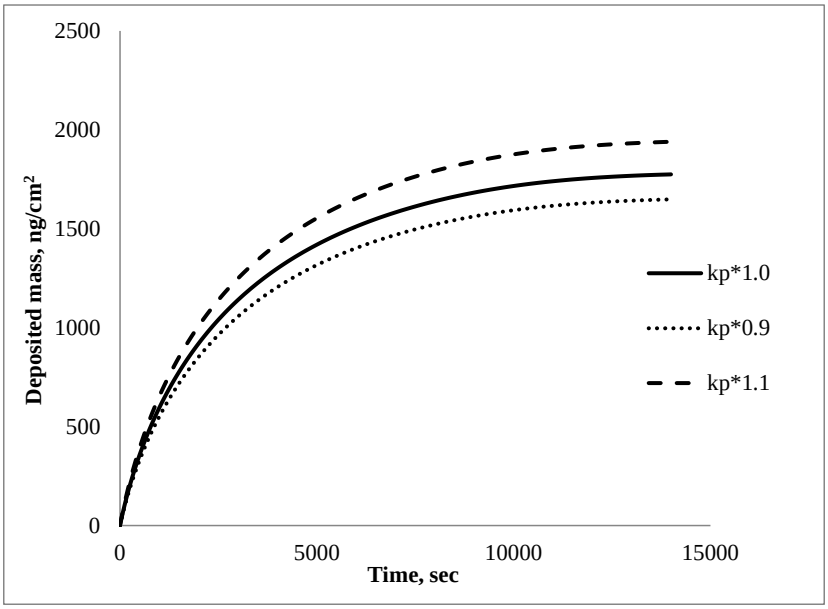

Figure 14. Effect of precipitation kinetic constant, k_p, on the deposited mass amount versus time.

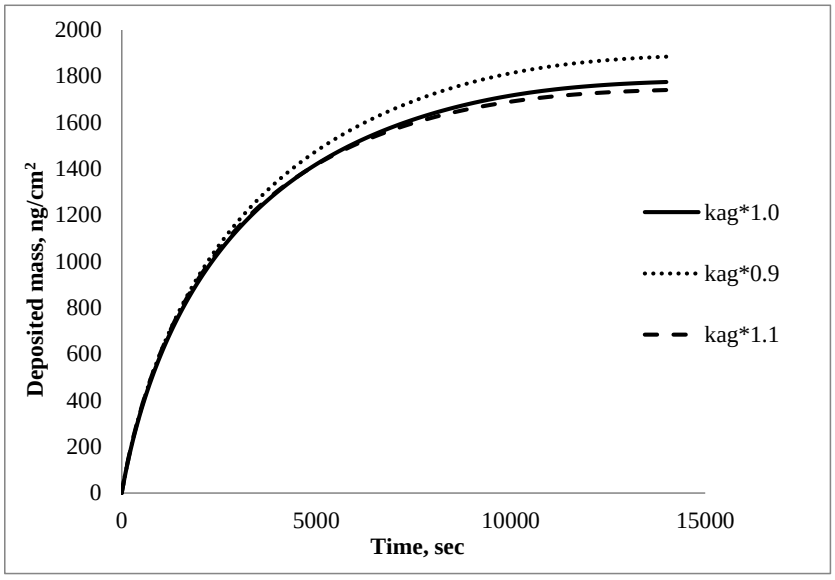

Figure 15. Effect of aggregation kinetic constant, k_{ag}, on the deposited mass amount versus time.

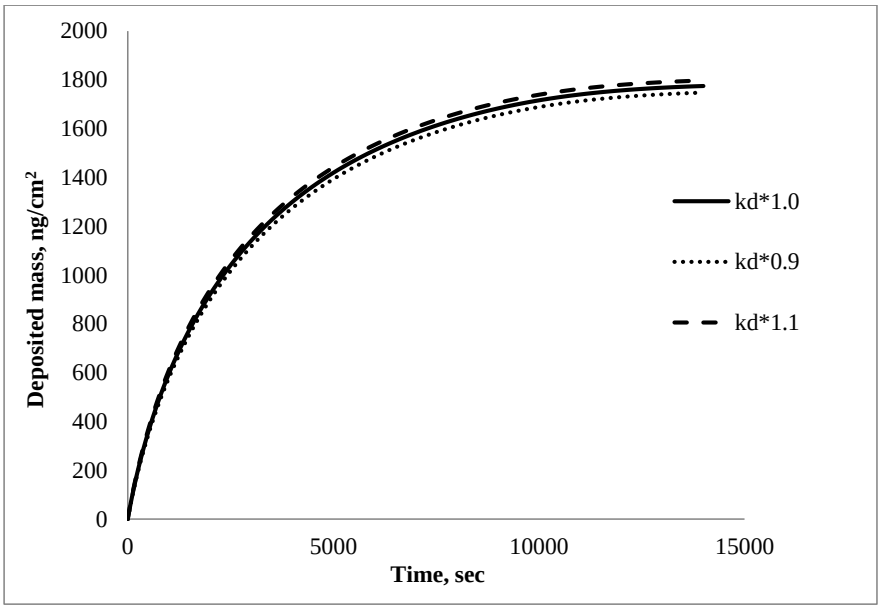

Figure 16. Effect of deposition kinetic constant, k_d, on the deposited mass amount versus time.

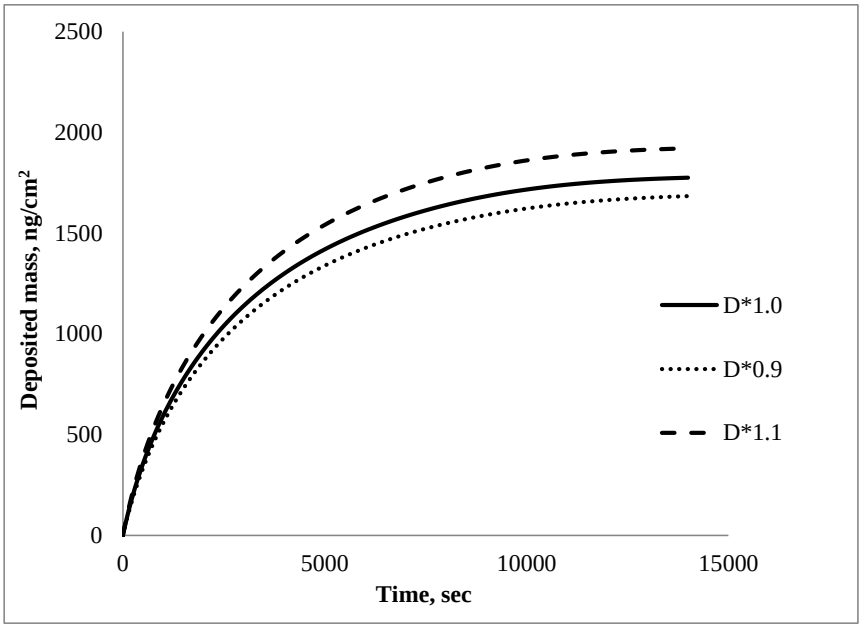

Figure 17. Effect of diffusion coefficient, *D*, on the deposited mass amount versus time.

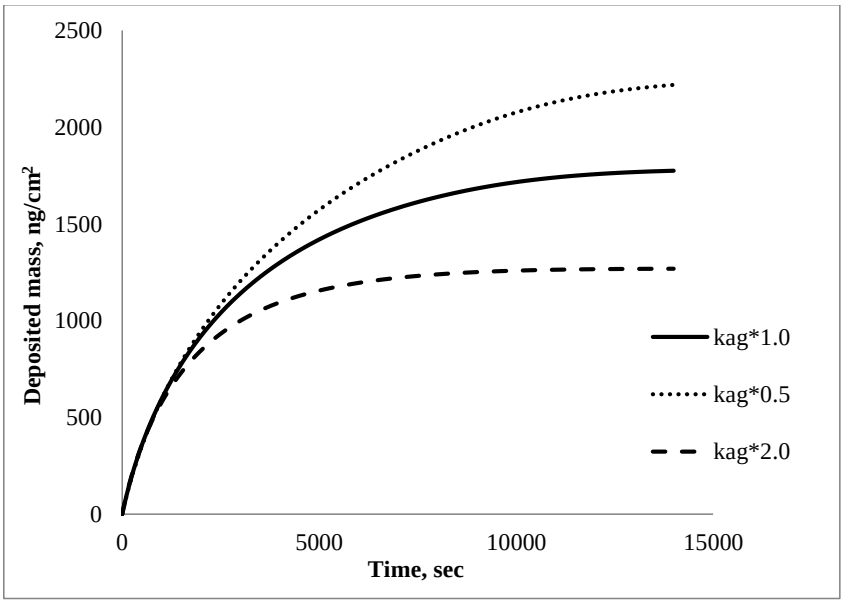

Figure 18. Effect on deposited mass amount versus time with a large change in aggregation kinetic constant, k_{ag}.

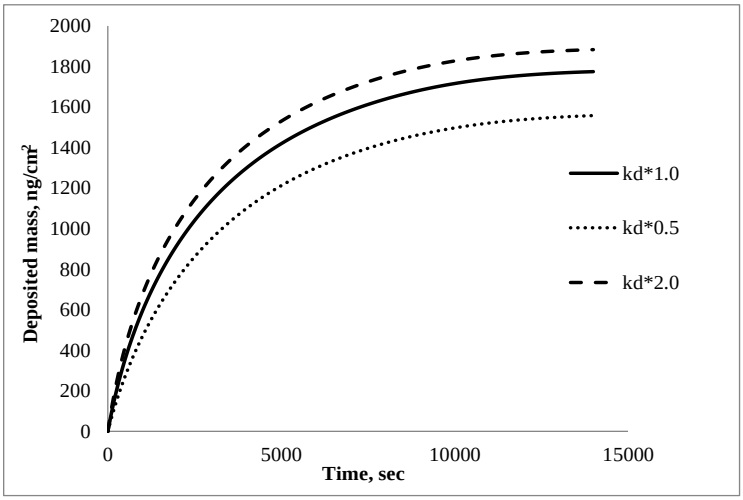

Figure 19. Effect on deposited mass amount versus time with a large change in kinetic constant of deposition, k_d.

4.7. Depositing Surface

To investigate the interaction between precipitated asphaltene from crude oil and pipeline material, carbon steel and iron oxide sensor crystals are used and compared to gold surface.

Many pipelines used for crude oil transport are made of carbon steel. Iron oxide presents the case of rust, and can provide an insight into change in asphaltene deposition behavior because of a rusted pipeline compared to a new steel pipeline.

Figure 20 shows the amount of deposited mass from 10 vol% crude oil + 90 vol% n-heptane system onto a gold, iron oxide and carbon steel sensor crystal surface versus time at 20 ^{o}C and 80 μl/min flow rate. It can be interpreted from Figure 20 that both carbon steel and gold surfaces represent more deposited mass in comparison to the iron oxide surface. At initial time, the amount of deposited mass on to a gold crystal is very close to the amount deposited on to a carbon steel surface. But, as time passes, gold sensor shows less amount of deposited mass in comparison to the carbon steel surface. Furthermore, the amount of mass deposited on an iron oxide surface is lesser than carbon steel sensor at all times.

For carbon steel surface, the modeling result is already presented in Figure 13 using the adjustable parameters shown in Table 4. To model the experimental data of Figure 20, for the surfaces of gold and iron oxide, the same parameters used for carbon steel case are used except for k_d. This is because the operating conditions are the same for all the cases except for the depositing surface. To get a close match with experimental data, the values of k_d used correspondingly for gold and iron oxide surfaces are 4.00E-8 and 2.50E-8 m/sec. Both represent a lower value in comparison to the k_d used for carbon steel sensor. Figures 21 and 22 show the experimental and modeling results for the amount of deposited mass versus time from a solution of 10 vol% crude oil + 90 vol% n-heptane on to gold and iron oxide surfaces, respectively.

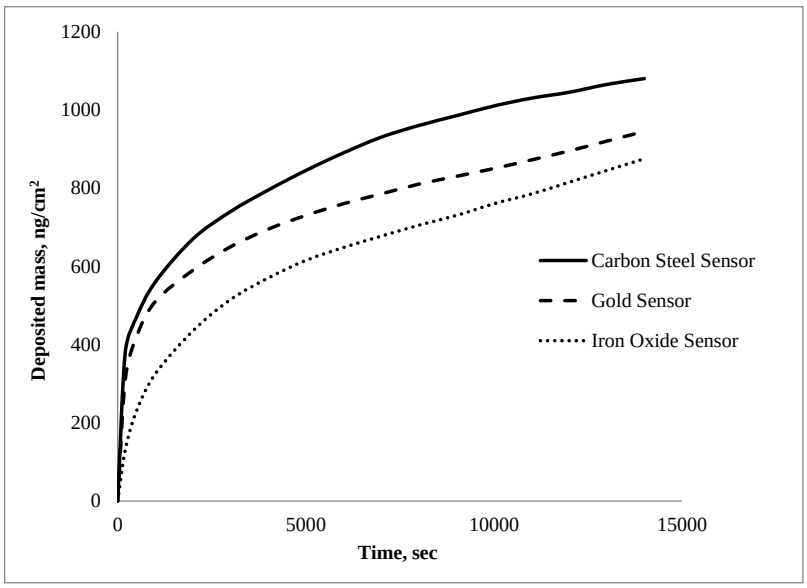

Figure 20. Amount of deposited mass from 10 vol% crude oil + 90 vol% n-heptane on different surfaces versus time at 20 ^{o}C and 80 µl/min flow rate.

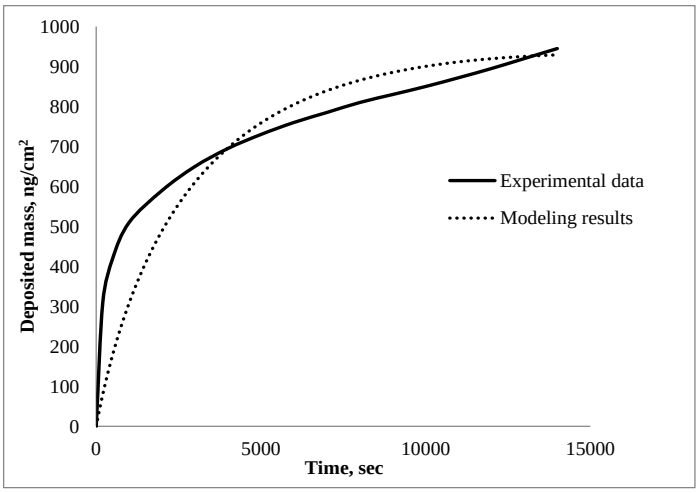

Figure 21. Experimental and modeling results for the amount of deposited mass versus time from a solution of 10 vol% crude oil + 90 vol% n-heptane on to a gold sensor at 20 ^{o}C and 80 µl/min flow rate.

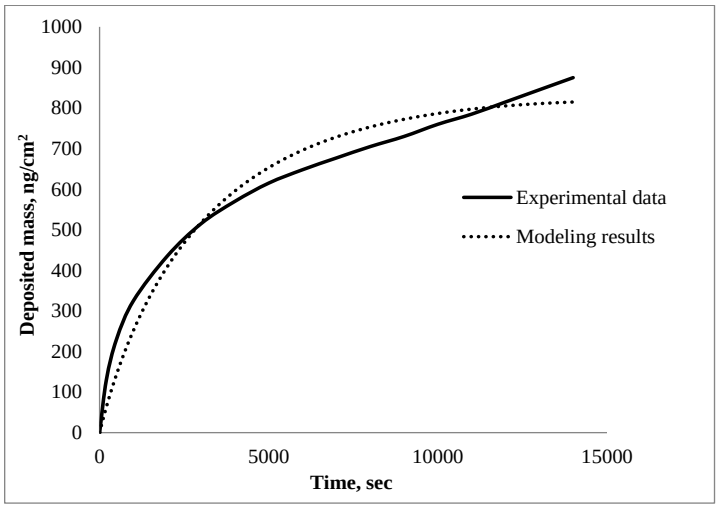

Figure 22. Experimental and modeling results for the amount of deposited mass versus time from a solution of 10 vol% crude oil + 90 vol% n-heptane on to an iron oxide sensor at 20 ^{o}C and 80 µl/min flow rate.

In this work, the precipitation, aggregation and deposition kinetic constants for the crude oil 'S' are adjusted to reproduce the asphaltene deposition experimental data obtained using a QCM-D setup. Using these adjusted kinetic constants, one can use the previously developed asphaltene deposition tool (ADEPT) by Kurup et al. to measure the asphaltene deposition profile in wellbores and pipelines in a fully predictive manner [11]. But, first a method needs to be developed for scaling the kinetic constant parameters from lab scale (QCM-D measurements) to field scale. Kurup et al. proposed a methodology for scaling up the deposition kinetic constant obtained from the capillary deposition experiments [11]. Scaling up the obtained kinetic constants from QCM-D experiments and linking between dynamic pipeline deposition and QCM-D deposition still needs a good deal of work.

Conclusions

In this article QCM-D experiments are performed to study the depositional aspects of asphaltene from crude oil systems. The frequency and dissipation changes because of the deposited layer and after accounting for liquid loading effect showed a viscoelastic behavior of the deposit. The following conclusions can be drawn from this study.

- For the system of 10 vol% crude oil + 90 vol% heptol under consideration, the precipitation onset happens near 75 vol% of heptane.
- Modeling of experimental data before asphaltene precipitation onset, for crude oil + heptol system, showed that the adsorption process is controlled by adsorption kinetics in initial times. The adsorption process at long time is governed by the diffusion and convective transfer. Rectangular adsorption isotherm is used, because all curves of deposited mass from crude oil reach equilibrium very soon.
- When the ratio of heptane to toluene increases, the amount of asphaltene deposited mass from the corresponding heptol solution increases up to the precipitation onset and decreases beyond that.
- After asphaltene precipitation, transport of asphaltene over the crystal in the flow module, may follow a multistep process, including precipitation, aggregation, diffusion, advection, and deposition. To model the amount of deposited mass beyond onset of asphaltene precipitation in a QCM-D experiment, a model is proposed with preliminary success for both model oil and real oil systems.
- From the sensitivity analysis of kinetic parameters, the value of k_p has a very significant impact on the amount of deposited mass, as compared to those of k_{ag} and k_d. Increasing k_p

increases the amount of deposited mass versus time and vice versa. Similar trend is observed for D and k_d, while an opposite trend is observed for change in k_{ag} and consistent with the mechanism.

- The effect of changes in k_{ag} on the deposited mass amount during initial time scale is very small while the effect of k_p and k_d is significant at all times.
- In the presence of rust (iron oxide), the amount of deposited mass decreases with respect to a carbon steel surface. Both carbon steel and gold surfaces represent more deposited mass in comparison to the iron oxide surface.
- For modeling of the experimental data with different surfaces, but under the same operating conditions, the only parameter which needs to be adjusted between different cases is the kinetic constant of deposition, k_d.

The work presented in this article can help in providing the deposition parameters for other asphaltene deposition simulators, and together with our previous article (Part 1) presents a complete experimental and modeling analysis of QCM-D asphaltene deposition.

Acknowledgement

This work is undertaken with the funding from DeepStar and R&D Oil Subcommittee of Abu Dhabi National Oil Company. The authors are also thankful to Matthew Dixon, Mark Poggi, Jianxin Wang, Qilin Li, Lisa Biswal, Maura Puerto, Francisco Vargas and Clarence Miller for experimental suggestions, lab space, access to equipment and helpful discussions.

Nomenclature

Δf : change in frequency

ΔD : change in energy dissipation

c : asphaltene primary particle's concentration

x : coordinate in the direction of flow

y : coordinate in the direction normal to flow

t : time

V : axial linear velocity

$\langle V \rangle$: average velocity

D : diffusion coefficient

c_i : concentration of asphaltene primary particles at initial conditions

c_0 : concentration of asphaltene in solution at inlet

c^{eq} : concentration of dissolved asphaltene at equilibrium

k : rate constant

r : rate

f_0 : fundamental resonant frequency

n : overtone number

ρ : density

v : shear wave velocity

μ : shear modulus

h : thickness

η : viscosity

Subscripts

x : coordinate in the direction of flow

y : coordinate in the direction normal to flow

p : precipitation

ag : aggregation

d : deposition

q : quartz

l : liquid

s : solvent

References

1. Tavakkoli, M.; Panuganti, S. R.; Vargas, F. M.; Taghikhani, V.; Pishvaie, M. R.; Chapman, W. G. *Energy & Fuels* **2014**, *28*, 1617-1628.
2. Abudu, A.; Goual, L. *Energy & Fuels* **2009**, *23*, 1237-1248.
3. Jaramillo, E.; Galeana, C. L.; Manero, O. *Energy & Fuels* **2006**, *20*, 1184-1196.
4. Akbarzadeh, K.; Ratulowski, J.; Lindvig, T.; Davies, T.; Huo, Z.; Broze, G. *SPE Annual Technical Conference and Exhibition*, 4-7 October **2009**, New Orleans, USA, SPE 124956.
5. Jamialahmadi, M.; Soltani, B.; Steinhagen, H. M.; Rashtchian, D. *International Journal of Heat and Mass Transfer* **2009**, *52*, 4624-4634.
6. Zhu, H.; Jing, J.; Che, J.; Li, Q.; Yu, X. *IEEE Int. Conf.*, 9-11 July **2010**, Chengdu, China.
7. Sileri, D.; Sahu, K.; Ding, H.; Matar, O. K. *International Conference on Heat Exchanger Fouling and Cleaning*, 14-19 June **2009**, Schladming, Austria.
8. Eskin, D.; Ratulowski, J.; Akbarzadeh, K.; Pan, S.; Lindvig, T. *International Conference on Multiphase Flow*, May 30-June 4 **2010**, Tampa, USA.
9. Vargas, F. M.; Creek, J. L.; Chapman, W. G. *Energy and Fuels* **2010**, *24*, 2294-2299.
10. Kurup, A. S.; Vargas, F. M.; Wang, J.; Buckley, J. S.; Creek, J. L.; Subramani, H. J.; Chapman, W. G. *Energy and Fuels* **2011**, *25*, 4506-4516.
11. Kurup, A. S.; Wang, J.; Subramani, H. J.; Buckley, J. S.; Creek, J. L.; Chapman, W. G. *Energy and Fuels* **2012**, *26*, 5702-5710.

12. Andersson, F. *Q-sense Webinar*, 10 December **2012**.

13. Filippov, L. K. *Journal of Colloid and Interface Science* **1995**, *174*, 32-39.

14. Panuganti, S. R.; Vargas, F. M.; Gonzalez, D. L.; Kurup, A. S.; Chapman, W. G. *Fuel* **2012**, *93*, 658-669.

15. Punnapala, S.; Vargas, F. M. *Fuel* **2013**, *108*, 417-429.

16. Panuganti, S. R.; Vargas, F. M.; Chapman, W. G. *Energy and Fuels* **2012**, *26*, 2548-2557.

17. Panuganti, S. R.; Tavakkoli M.; Vargas, F. M.; Gonzalez, D. L.; Chapman, W. G. *Fluid Phase Equilibria* **2013**, *359*, 2-16.

18. Kanazawa, K. K.; Gordon II, J. G. *Analytical Chemistry* **1985**, *57*, 1770-1771.

19. Tavakkoli, M.; Panuganti, S. R.; Taghikhani, V.; Pishvaie, M. R.; Chapman, W. G. *Fuel* **2014**, 117, 206−217.

20. Rajagopal, K; Silva, S. M. C. *Brazilian Journal of Chemical Engineering* **2004**, *21*, 601-609.